Progress In Electromagnetics Research, PIER 87, 167–182, 2008

A NEW METHOD TO EXTRACT THE POLARIMETRIC PARAMETERS IN IMAGING RADARS

B. Zakeri, A. Ghorbani, and H. Amindavar

Department of Electrical Engineering
Amirkabir University of Technology (Tehran Polytechnic)
Tehran, Iran

Abstract—In this paper, a statistical approach to evaluate randomly rough surfaces (RRS) in an inverse scattering problem is presented. Whereas in these investigations the roughness criterions possess random variables, the use of deterministic techniques such as the target decomposition (TD) can not be useful by itself as a tool of analysis. In these conditions, a statistical approach is essentially required to evaluate the target parameters. The goal of this study is the estimation of the polarimetric signatures, such as the scattering mechanism α and the entropy H, via a novel approach including the combination of TD and a new statistical model. To validate our work, SAR data sets, provided by the European Space Agency (ESA), are analyzed and compared with the simulation results.

1. INTRODUCTION

In many applications, such as environmental and earth observations, the polarimetric radars are powerful tools for retrieving quantitative physical information [1–3]. In these frameworks, the bridge between radar measurements and physical parameters can be organized by target decomposition (TD) methods [4]. Among these approaches, the target decomposition method based on the eigenvector analysis (EV-TDM) is one of the most appropriate techniques to achieve data interpretations [5].

Recently in inverse scattering problems, the scattering mechanism of randomly rough surfaces (RRS) has attracted significant attention [6–8]. These surfaces are classified in terms of the permittivity and geometrical shapes. In these contexts, the polarimetry plays an important role, as it allows a direct or indirect separation of roughness effects, and several inversion models are based on the use of full

polarimetric images [9–12]. In the remote sensing of natural surfaces, the roughness criterions, i.e., ks and kl, are significant parameters for the estimation of the polarimetric signatures. Whereas these parameters possess random variables, deterministic techniques, proposed in the literatures, can not be useful alone as tools of analysis. This means that the use of a proper stochastic approach to assess natural targets is unavoidable. For this aim a number of statistical models, such as the Wishart distribution (WD), can be utilized [13, 14]. Consequently the aim of this work is the combination of a deterministic technique and a new stochastic model, i.e., TD and modified Wishart distribution (MWD), to present the physical interpretation of natural targets.

This paper is organized as follows; first in Section 2 a systematic solution for calculating of the scattered fields upon RRS is addressed and then two polarimetric signatures are introduced for the physical interpretation of target parameters. Furthermore, a new statistical model to extract target parameters is proposed in Section 3. Moreover in Section 4, several scattering mechanisms of RRS are simulated with respect to the effective parameters. Finally to validate our work, SAR data sets classified by the European Space Agency (ESA) are analyzed and compared with the simulation results.

2. THEORY

2.1. RRS Under Study

In this paper, to assess distributed targets such as natural scatterers, we consider an arbitrary RRS as shown in Figure 1(a). This structure possesses an arbitrary surface, i.e., $S = L \times L$, subdivided into many appropriate spaces Δx and $\Delta y \leq 0.1\lambda$ as illustrated in Figure 1(b). Each section denotes a pyramidal configuration and its surfaces have the local angles with respect to the main surface as can be seen from Figure 1(c). Usually these angles have the uniform distribution with $\delta_1 < \pi/2$ as plotted in Figure 1(d). The surface rms height s and the correlation function are extracted from surface under study and compared with the theory as presented in Figure 2. In this structure, the correlation length l, in S-band frequency with $\lambda = 10\,\text{cm}$, is 76 cm as well as the roughness criterions are $ks = 5.48$ and $kl = 47.75$ denoting a very rough surface. In the next section, the scattered fields of this surface are calculated by using the Kirchhoff approximation (KA) method.

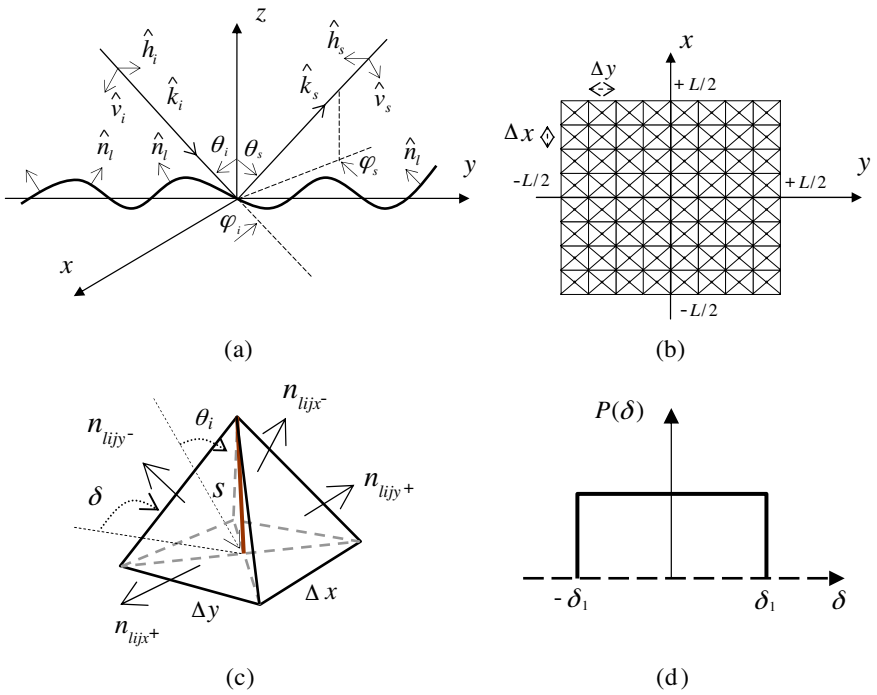

Figure 1. Structure under study. (a) RRS in a proper coordinate system. (b) Fragmented surface with appropriate spaces Δx and $\Delta y \leq 0.1\lambda$. (c) Local unit vectors on the walls. (d) Distribution of the angles.

2.2. Scattered Fields Calculation

The scattering problem of EM waves upon RRS is still not satisfactorily solved and no exact closed-form solutions exist so far. But, for many practical applications, approximate solutions are sufficient [15–17]. In the field of radar remote sensing, various approximate methods for wave scattering at rough surfaces have been developed [18, 19]. Among these solutions, the most common approximate method has been the Kirchhoff approximation (KA). This method is valid when the surface roughness dimensions are large compared to the wavelength. In this case, the scattering at a point on the surface may be considered as scattering at the tangential plane to this point. Whereas in this study, we deal with various RRS including high rms heights, the use of this method is feasible. It is assumed that the total field at any point on the surface can be computed as if the incident wave is impinging upon

an infinite plane tangent to the point.

According to Stratton and Chu's formula [20], the total scattered field can be calculated as:

$$\vec{E}^s = \frac{-j\hat{k}_s e^{-jk_s R_o}}{4\pi R_0} \sum_{ij} \left[\vec{E}_{\tan \cdot ij} - \eta_0 \hat{k}_s \times \vec{H}_{\tan \cdot ij} \right] e^{j\hat{k}_s \cdot \vec{r}} \Delta s \qquad (1)$$

where $\mathbf{E}_{\tan}$ and $\mathbf{H}_{\tan}$ are the tangential electric and magnetic fields and K_s, η_0 and R_0 are the wave number, intrinsic impedance and range from the center of the illuminated area to the point of observation respectively. Basically in the fully polarimetric radars, the incident wave contains two polarized waves such as the horizontal and vertical linear polarizations, i.e., $\mathbf{E}_i = E_{ih}\mathbf{h}_i + E_{iv}\mathbf{v}_i$ where i is an incidence index. In this case, the horizontal and vertical unit vectors with respect to the plane of incidence can be defined as follows:

$$\hat{h}_i = \frac{\hat{k}_i \times \hat{z}}{\left| \hat{k}_i \times \hat{z} \right|}, \qquad \hat{v}_i = \hat{k}_i \times \hat{h}_i \qquad (2)$$

where $k_i = 2\pi/\lambda$ denotes the incident wave number which its vector is defined by:

$$\hat{k} = \frac{2\pi}{\lambda} \left[-\sin(\theta_i)\cos(\varphi_i)\hat{x} + \sin(\theta_i)\sin(\varphi_i)\hat{y} - \cos(\theta_i)\hat{z} \right] \qquad (3)$$

In the surface scattering, a RRS located in a proper coordinate system has azimuthal symmetry [4] as shown in figure 1(a). This means that the angle φ_i is not important and can be canceled, i.e., $\varphi_i = 0$. In this condition, after substituting (3) in (2), the horizontal and vertical unit vectors are reduced as follows:

$$\hat{h}_i = \hat{y} \qquad (4)$$

$$\hat{v}_i = -\cos(\theta_i)\hat{x} + \sin(\theta_i)\hat{z} \qquad (5)$$

In addition, the unit vector on the pyramid surfaces is given as:

$$\hat{n}_l = \frac{-Z_x\hat{x} - Z_y\hat{y} + \hat{z}}{\sqrt{Z_x^2 + Z_y^2 + 1}}, \quad Z_x = \tan(\delta_x), \quad Z_y = \tan(\delta_y) \qquad (6)$$

where δ_x and δ_y are local angles with respect to the main surface in x and y directions respectively. Therefore the normal unit vectors on the pyramid surfaces, i.e., $\boldsymbol{n}_{lijx-}$, $\boldsymbol{n}_{lijx+}$, $\boldsymbol{n}_{lijy-}$ and $\boldsymbol{n}_{lijy+}$, are defined

by:

$$\hat{n}_{ijx^+} = \frac{1}{D_{ij}}\left[\frac{2Z(i,j)}{\Delta x}\hat{x}+\hat{z}\right], \quad \hat{n}_{ijx^-} = \frac{1}{D_{ij}}\left[\frac{-2Z(i,j)}{\Delta x}\hat{x}+\hat{z}\right] \quad (7)$$

$$\hat{n}_{ijy^+} = \frac{1}{D_{ij}}\left[\frac{2Z(i,j)}{\Delta y}\hat{y}+\hat{z}\right], \quad \hat{n}_{ijy^-} = \frac{1}{D_{ij}}\left[\frac{-2Z(i,j)}{\Delta y}\hat{y}+\hat{z}\right] \quad (8)$$

In these formulas, $Z(i,j)$ is the rms height s for an arbitrary point on the surface and D_{ij} is defined by:

$$D_{ij} = \left(\frac{4Z^2(i,j)}{\Delta x^2}+1\right)^{1/2} \quad (9)$$

Therefore the local tangential fields can be obtained as:

$$\begin{aligned}\vec{E}_{\tan\cdot ijx\pm} &= \hat{n}_{ijy\pm}\times[E_{ih}(1+\Gamma_h)\hat{y} \\ &\quad +E_{iv}(1+\Gamma_v)(-\cos(\theta_i)\hat{x}+\sin(\theta_i)\hat{z})] \quad (10)\\ \vec{E}_{\tan\cdot ijy\pm} &= \hat{n}_{ijy\pm}\times[E_{ih}(1+\Gamma_h)\hat{y} \\ &\quad +E_{iv}(1+\Gamma_v)(-\cos(\theta_i)\hat{x}+\sin(\theta_i)\hat{z})] \quad (11)\end{aligned}$$

After substituting (7) and (8) in the above formulas, the tangential electric fields on the each surface are obtained by:

$$\begin{aligned}\vec{E}_{\tan\cdot ijx\pm} &= \frac{E_{ih}(1+\Gamma_h)}{D_{ij}}\left[\frac{\pm 2Z(i,j)}{\Delta x}\hat{z}-\hat{x}\right] \\ &\quad +\frac{E_{iv}(1+\Gamma_v)}{D_{ij}}\left[\frac{\mp 2Z(i,j)\sin(\theta_i)}{\Delta x}-\cos(\theta_i)\right]\hat{y} \quad (12)\\ \vec{E}_{\tan\cdot ijy\pm} &= \left(\pm\frac{2Z(i,j)E_{iv}(1+\Gamma_v)}{\Delta y}\sin(\theta_i)-\frac{E_{ih}(1+\Gamma_h)}{D_{ij}}\right)\hat{x} \\ &\quad -\frac{E_{iv}(1+\Gamma_v)}{D_{ij}}\cos(\theta_i)\hat{y}\pm\frac{2Z(i,j)E_{iv}(1+\Gamma_v)}{D_{ij}\Delta y}\cos(\theta_i)\hat{z} \quad (13)\end{aligned}$$

where Γ_h and Γ_v are the horizontal and vertical reflection coefficients respectively which can be obtained from the surface permittivity and the local angles [20]. By a similar way, the tangential magnetic field, i.e., $\mathbf{H}_{\tan ijx+-}$ and $\mathbf{H}_{\tan ijy+-}$, on each surface can be calculated and substituted in (1) for finalizing the scattered field calculation.

Due to the polarization diversity technique, the scattering coefficients, i.e., S_{hh}, S_{hv}, S_{vh} and S_{vv}, can be found by the contribution of the horizontal and vertical incident fields. These coefficients organize the scattering matrix S and the covariance

matrix C to present the polarimetric signatures denoting the physical interpretation of polarimetric data [4]. In the next section, these signatures are briefly introduced and a new statistical model is proposed for the estimation of them.

3. PHYSICAL INTERPRETATION

3.1. Polarimetric Signatures

In order to interpret the polarimetric matrices, i.e., the scattering matrix S and the covariance matrix C, there are two polarimetric signatures which are directly extracted by the eigenvalues analysis of the covariance matrix [4, 5]. These parameters are the scattering mechanism α and the entropy H which are defined as:

$$\alpha = \sum_{i=1}^{3} p_i \alpha_i, \quad H = -\sum_{i=1}^{3} p_i \log_3(p_i), \quad p_i = \frac{\lambda_i}{\lambda_1 + \lambda_2 + \lambda_3} \tag{14}$$

where λ_1, λ_2 and λ_3 are the eigenvalues of the covariance matrix and p_i and α_i are the probability and the scattering mechanism of λ_i respectively. The α-angle varies between zero and 90 degrees corresponding to the type of scatterers. The entropy can be interpreted as a measure of the randomness of the scattering process. For example for smooth surfaces, the entropy H becomes zero and increases with surface roughness. The combination of these parameters provides a useful physical representation namely the classification plane H-α. By using this plane, the eight usable classes, denoting an individual type of the scattering mechanism independent on particular data set, can be suggested [4]. Whereas these parameters possess random variables in the scattering of natural targets, a statistical assessment is essentially required. In the next section, a new statistical model is briefly described to extract eigenvalues matrix.

3.2. A New Statistical Model

As previously mentioned, there are several statistical models for estimating of the polarimetric matrices in inverse problems. Among these models the Wishart distribution (WD) is a robust technique which is useful for multidimensional synthetic aperture radars (MD-SAR). In the m-dimensional SAR, the target vectors [4] possess m independent elements and therefore their polarimetric matrices have m^2 elements. Whereas these elements may not be correlated, we must be used a general form of WD. In the case of the three dimensional SAR

(3D-SAR), i.e., the mono-static radar or backward scattering alignment (BSA), the target vectors have four elements, such as S_{11}, S_{12}, S_{21} and S_{22}, which are extremely correlated [4], i.e., $S_{12} = S_{21}$. In this condition, the use of the general form of WD is a very complicated problem and therefore we propose a modified Wishart distribution (MWD) for estimating of the covariance matrix C in the form of:

$$P_{C_{est}}(C_{est}) = \frac{N^{3N} \left|C_{est}\right|^{N-3} e^{tr(-NC_{true}^{-1}C_{est})}}{\pi^3 \left|C_{true}\right|^{N} \prod_{i=1}^{3} \Gamma(N-i+1)} \tag{15}$$

where $Tr(\cdot)$ and $\Gamma(\cdot)$ denote the trace and gamma functions respectively and the parameter N shows the number of looks in the scanning process. In (15), C_{true} and C_{est} possess the true eigenvalues l_1, l_2, l_3 and estimated eigenvalues λ_1, λ_2, λ_3. By using this model, the estimated eigenvalues can be correctly extracted from the true eigenvalues. For instance while the true eigenvalue l_1 is 3, the probability density function (pdf) of the eigenvalue λ_1 with respect to the parameter N, i.e., $N = 1, 2, \ldots, 60$, is shown in Figure 3. As can be seen from this figure, the estimated eigenvalue λ_1 asymptotically approaches to the true value l_1 when N is increased. This procedure shows that the eigenvalues are correctly estimated when the number of looks becomes very large. Furthermore the pdf of the estimated eigenvalue λ_1 is represented in Figure 4 with respect to the scattering mechanism α for a typical RRS which is introduced in Figure 2. $P_{\lambda 1}(\lambda_1)$ presents a Bragg surface scattering and a dipole effect when the α-angle approaches zero and 90 degrees respectively. From these results we can conclude that the sample eigenvalues can be correctly estimated by using the proposed model. In the next section, the eigenvalues of several types of RRS as well as their polarimetric signatures are simulated.

4. SIMULATION RESULTS

The simulation is presented with respect to the incidence angle θ_i and the surface permittivity ε_r. In order to evaluate the behavior of the permittivity, the α-angle is plotted versus surface slope in Figure 5. In small slopes, the α-angle approaches to less than 5 degrees denoting a Bragg surface scattering as shown in Figure 5(a). For the surface including large permittivity, the α-angle is independent of the surface slope and approaches zero denoting a fully polarized wave. It is worth to note that this condition occurs when the bare soil is exceedingly moisturized. In the case of large slopes and small

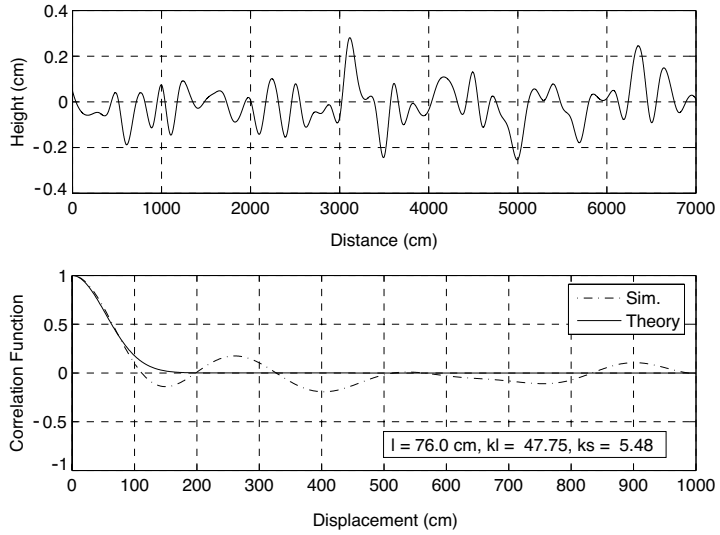

Figure 2. Surface profile and correlation function for RRS under study.

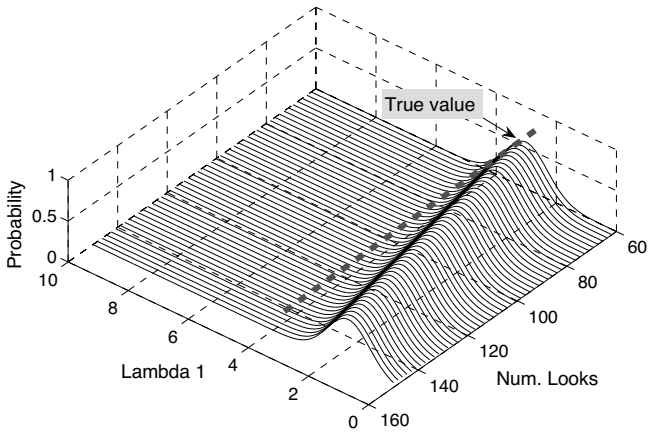

Figure 3. Probability of the sample eigenvalue λ_1.

permittivity, the scattering mechanism is independent of the surface slope and is very close to 90 degrees denoting a dipole scattering as illustrated in Figure 5(b).

Furthermore the behavior of the incidence angle shows that the α-angle for very small slopes denotes a dipole effect with increasing θ_i

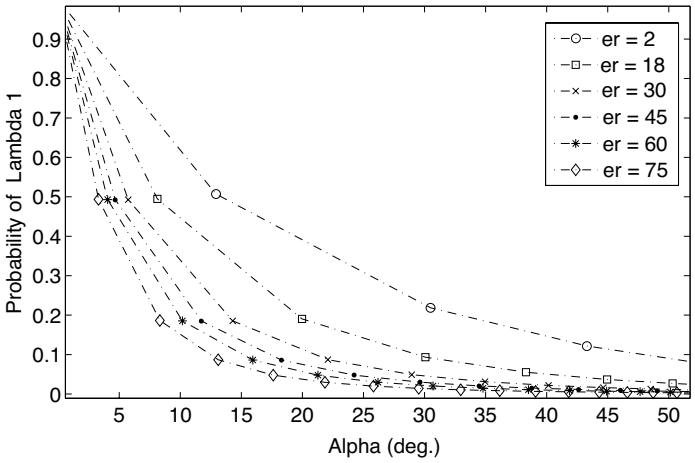

Figure 4. Probability density function with respect to the scattering mechanism for a typical RRS.

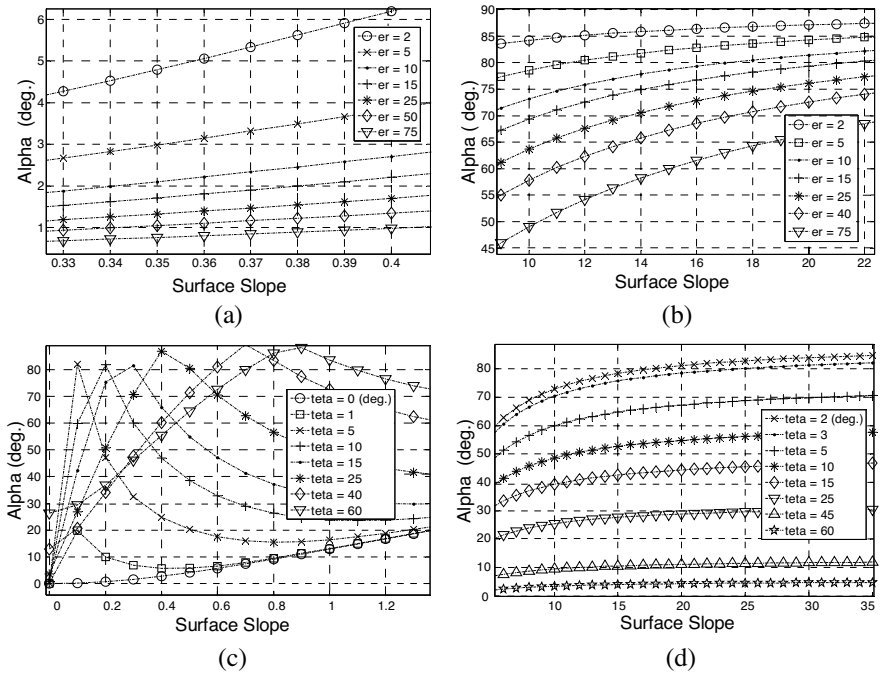

Figure 5. Scattering mechanism assessments versus surface slope for several types of RRS.

as illustrated in Figure 5(c). With regarding to Figure 5(d) for very large slopes, the α-angle, which is extremely dependent on the angle of incidence, is fixed versus the surface slope. The α-angle approaches to less than 5 degrees when the angle of incidence is a large value. These results clearly indicate that the scattering of RRS is classified as various known scattering mechanisms which are easily recognized from each other. To validate these results, real data sets including several different kinds of the scattering mechanisms are utilized in the next section.

5. SAR DATA

In the former section, the α-angle for various types of RRS has been discussed. In order to validate of these results, we have applied real data set from several test fields. These regions denote a number of suitable scattering mechanisms, such as the Bragg, dipole, multiple and double bounce scattering, located in the San Francisco Bay and the Foulum areas. The data set are extracted by SIR/C-AIR/SAR and EMISAR sensor including a STK-MLC format and no header as well as a resolution of 77 rows $\times$ 99 columns.

Figure 6 illustrates the H-α and the segmented planes of the eigenvalues λ_1, λ_2 and λ_3 for the San Francisco Bay areas. The data sets show that the α-angle approaches 10 degrees and the entropy has a value very close to zero for sea surface. Moreover the scattering mechanism has features with a statistical behavior in agreement with the following parameters: mean = 10.06, median = 9.844, mode = 9.844, std = 2.832 and max = 23.91 degrees. It is interesting to see from Figure 6(a) that the bridge is clearly distinguishable from sea areas which exhibit a mechanism compatible to the surface scattering.

Moreover Figure 7 represents another polarimetric measurement and physical interpretation for the same data sets. The probability density function (pdf) of the dominant eigenvalue λ_1 is represented at nine vertical scans over the bridge. The averaged value of this probability approaches 0.95 and 0.35 for the surface of the bridge and sea respectively. These results signify that the probability of the target detection is higher than 95 percents.

For the Foulum regions, the histogram of the α-angle extracted from four types of regions, such as lake, bare soil, forest and vegetated surface, are presented in Figure 8. It is worth to notice that each scattering mechanism has an individual feature denoting a significant difference. The average of the α-angle for the lake surface is 30.03 degrees unlike the scattering of a sea surface as illustrated in Figure 8(a). Because of the dissimilarity between sea and lake waters,

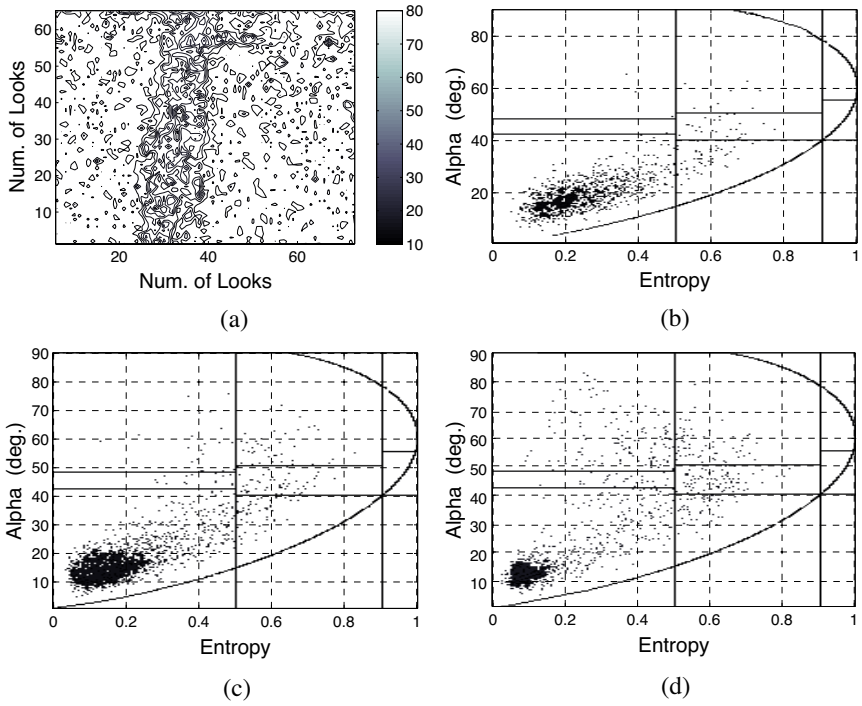

Figure 6. Polarimetric parameters of the San Francisco Bay areas. (a) α-angle for the bridge area. (b) Segmented plane of λ_1. (c) Segmented plane of λ_2. (d) Segmented plane of λ_3.

caused by fluctuations of the permittivity, this difference occurs. As shown in Figures 8(b)–(d), the averaged values of this mechanism are 37.38, 48.67 and 40.98 degrees for the bare soil, forest areas and vegetated surface respectively. These values signify that the forest represents a multiple scattering and the bare soil and the vegetated surface have similar mechanisms. Because of this similarity for the bare soil and vegetated surface, a proper recognition algorithm cannot be easily implemented. This problem can be considered for future works.

Moreover a quantitative assessment of the scattering mechanism is presented in Table 1. The α-angle is extracted with respect to the number of looks N. These angles for the bare soil are 34.40, 37.98, 37.99 and 39.40 when N is 126, 544, 1312 and 2736 respectively. This process shows that the α-angle asymptotically approaches to the true value with increasing N. Usually in these investigations the introduction of a quantitative parameter namely the differential ratio

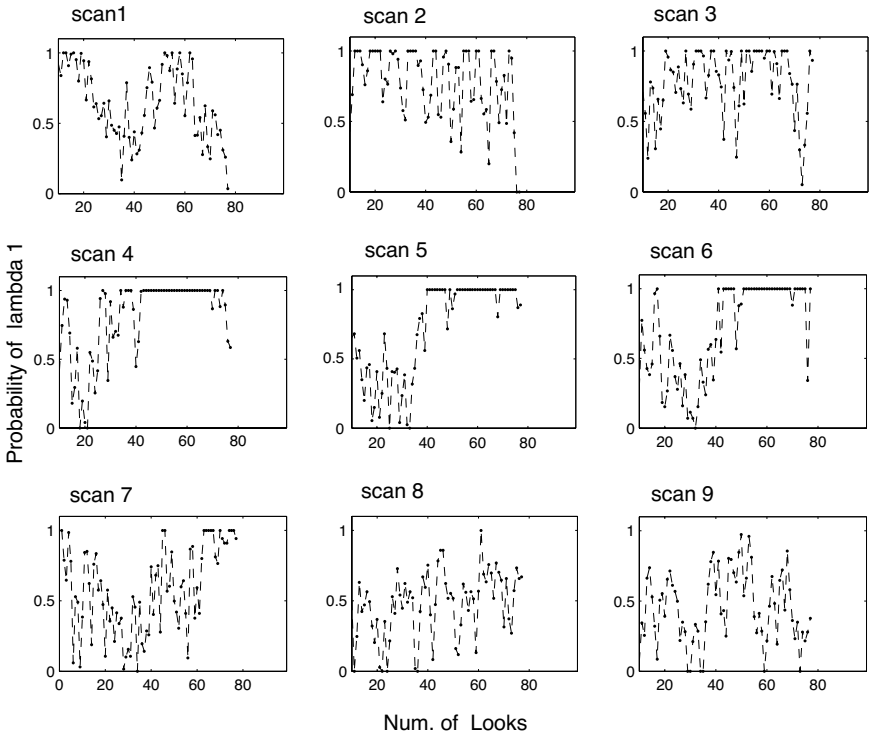

Figure 7. Probability of the dominant eigenvalue λ_1 in several scans for around the bridge.

ΔR can be sensible. This parameter is defined in the form of:

$$\Delta R = \frac{\alpha_{asy} - \alpha_{ini}}{\alpha_{asy}} \times 100 \tag{16}$$

where α_{asy} and α_{ini} are the final and initial values of the scattering mechanisms respectively. This parameter is arranged in Table 1 for four types of the scattering mechanisms. It is interesting to see that ΔR for the bare soil, forest area, lake and vegetated surface are 12.6%, 0.75%, 6.3% and 4.3% respectively. At here a significant difference can be realized from these values. The first is that the number of iterations, i.e., N, is different for each scattering mechanism. The second is that for the forest, the number of N is small denoting a fast iterative algorithm unlike the scattering of the bare soil. As a result, we can observe that ΔR can be a useful parameter to implement a recognition algorithm in inverse problems.

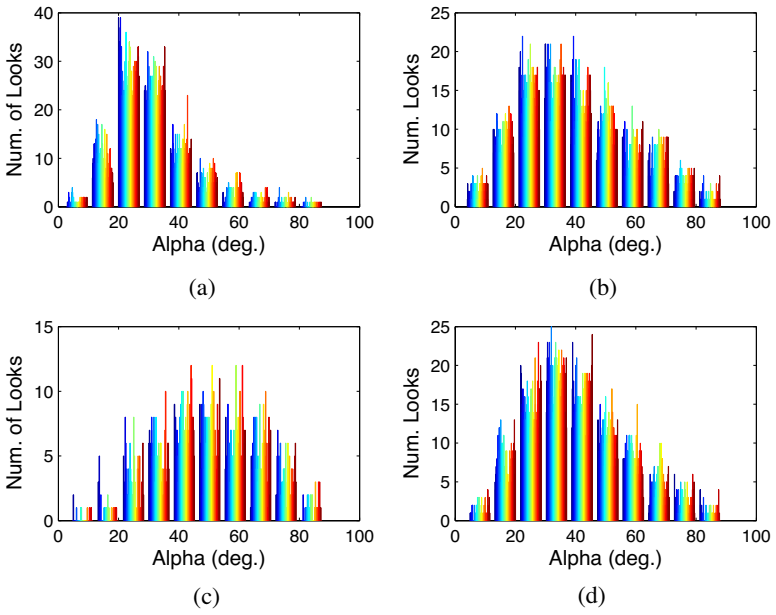

Figure 8. Histogram of the α-angle for several types of scatterers. (a) Lake. (b) Bare soil. (c) Forest. (d) Vegetated surface.

Table 1. α-angles for several types of scattering mechanisms with respect to number of looks.

Test fields							
Bare soil		forest area		lake surface		vegetated surface	
N	α (deg.)	N	α (deg.)	N	α (deg.)	N	α (deg.)
126	34.40	180	50.40	410	29.14	553	41.96
390	37.17	312	48.65	1230	29.70	869	41.69
544	37.98	720	48.20	1804	30.01	1116	40.85
1312	37.99	1014	48.09	3280	30.20	1612	40.30
2736	39.40	1443	48.02	5248	31.10	1659	40.10
Averaged values							
1021	37.38	733	48.67	2394	30.03	1161	40.98
ΔR = 12.6 %		ΔR = 0.75 %		ΔR = 6.3 %		ΔR = 4.3 %	

6. CONCLUSIONS

In this paper, we have studied the polarimetric signatures such as the α-angle and entropy in the scattering of EM waves upon RRS. For this aim, a new statistical model to estimate these signatures has been proposed. After extracting the scattering coefficients via polarization diversity, the polarimetric signatures have been simulated for various RRS and compared with real data to validate the proposed model.

In the simulation scheme, the results of RRS have been presented with respect to the incidence angle θ_i and surface permittivity ε_r. We have observed that for very large incident angle, this mechanism is independent of the surface slope and approaches zero denoting a fully polarized wave. For very large slopes, this mechanism, which is extremely dependent on the angle of incidence, is fixed versus the slope. The results clearly indicate that the scattering of RRS can be classified by the known mechanisms which are usually observed in remote sensing applications.

The real data sets indicate that the histogram of the α-angle for the bare soil, forest areas and vegetated surface denotes a significant difference. It is worth to notice that the bare soil and vegetated surface have similar mechanisms which their recognition is very difficult. This problem can be considered for future works.

A quantitative assessment of the scattering mechanisms indicates that the α-angle asymptotically approaches to the true value with respect to increase the number of looks which is an important parameter in the data processing. In addition, the quantitative parameter ΔR indicates that the iteration number is dependent on the type of the scattering mechanism. Consequently ΔR can be utilized as a useful parameter to introduce a recognition mechanism in inverse problems. Finally it is possible to conclude that the technique proposed in this study is an efficient method for the target recognition in SAR applications.

ACKNOWLEDGMENT

In this study, SAR data set is provided by the European Space Agency (ESA). The authors would like also to thank Martin Suess (ESA) and Alberto Moreira (DLR) for their many constructive discussions and helpfull comments.

REFERENCES

1. Storvold, R., E. Malnes, Y. Larsen, and K. A. Hgda, "SAR remote sensing of snow parameters in Norwegian areas current status and future perspective," *Journal of Electromagnetic Waves and Applications*, Vol. 20, No. 13, 1751–1759, 2006.
2. Chen, X., D. Liang, and K. Huang, "Microwave imaging 3-D buried objects using parallel genetic algorithm combined with FDTD technique," *Journal of Electromagnetic Waves and Applications*, Vol. 20, No. 13, 1761–1774, 2006.
3. Vulpiani, G. and F. S. Marzano, "Polarimetric weather radar retrieval of raindrop size distribution by means of a regularized artificial neural network," *IEEE Geosci. and Remote Sens. Letters*, 44–11, 2006.
4. Cloude, S. R. and E. Pottier, "A review of target decomposition theorems in radar polarimetry," *IEEE Trans. Goesci. Remote Sensing*, Vol. 34, No. 2, 498–518, 1996.
5. Pottier, E. and J. S. Lee, "Unsupervised classification of Pol-SAR images based on the complex Wishart distribution and the H/A/α polarimetric decomposition theorem," *Proc. EUSAR, Munich*, Germany, 2000.
6. Hajnsek, I., E. Pottier, and S. R. Cloude, "Inversion of surface parameters from polarimetric SAR," *IEEE Trans. Goesci. Remote Sensing*, Vol. 41, No. 4, 727–744, 2003.
7. Wang, P. and Y. Xie, "Scattering and radiation problem of surface/subsurface junction structure with multilevel fast multiple algorithm," *Journal of Electromagnetic Waves and Applications*, Vol. 20, No. 15, 2189–2200, 2006.
8. Bourlier, C. and G. Berginc, "Microwave analytical backscattering models from randomly rough anisotropic sea surface comparison with experimental data in C and Ku-bands," *Progress In Electromagnetics Research*, PIER 37, 31–78, 2002.
9. Kuo, C. and M. Moghaddam, "Scattering from multilayer rough surfaces based on the extended boundary condition method and truncated singular value decomposition," *IEEE Trans. on Antennas and Propagation*, Vol. 54, No. 10, Oct. 2006.
10. Rigling, B. D. and R. L. Moses, "Three-dimensional surface reconstruction from multistatic SAR images," *IEEE Trans. on Image Processing*, Vol. 14, No. 8, 2005.
11. Fung, A. K. and N. C. Kuo, "Backscattering from multi-scale and exponentially correlated surfaces," *Journal of Electromagnetic Waves and Applications*, Vol. 20, No. 1, 3–11, 2006.

12. Charnotskii, M. I., "Wave scattering by periodic surface at low grazing angles: Single grazing mode," *Progress In Electromagnetics Research*, PIER 26, 1–41, 2000.
13. Martinez, C. L. and E. Pottier, "Statistical assessment of eigenvector-based target decomposition theorems in radar polarimetry," *IEEE Trans. Goesci. Remote Sensing*, Vol. 43, No. 9, 2005.
14. Lee, J. S., M. R. Grunes, D. L. Schuler, E. Pottier, and L. F. Famil, "Scattering-model-based speckle filtering of polarimetric SAR data," *IEEE Trans. Geosci. Remote Sensing*, Vol. 44, No. 1, 2006.
15. Granet, G., K. Edee, and D. Felbacq, "Scattering of a plane wave by rough surfaces: A new curvilinear coordinate system based approach," *Progress In Electromagnetics Research,* PIER 37, 235–250, 2002.
16. Cocheril, Y. and R. Vauzelle, "A new ray-tracing based wave propagation model including rough surfaces scattering," *Progress In Electromagnetics Research*, PIER 75, 357–381, 2007.
17. Baudier, C. and R. Dusseaux, "Scattering of an E-polarized plane wave by one-dimensional rough surfaces: Numerical applicability domain of a Rayleigh method in the far-field zone," *Progress In Electromagnetics Research*, PIER 34, 1–27, 2001.
18. Berginc, G., "Small-slope approximation method: A further study of vector wave scattering from two-dimensional surfaces and comparison with experimental data," *Progress In Electromagnetics Research*, PIER 37, 251–287, 2002.
19. Ishimaru, A., C. Le, Y. Kuga, L. A. Sengers, and T. K. Chan, "Polarimetric scattering theory for high slope rough surface," *Progress In Electromagnetics Research*, PIER 14, 1–36, 1996.
20. Ulaby, F. T., R. K. Moore, and A. K. Fung, *Microwave Remote Sensing*, Vol. 2, Artech House, Norwood, MA, 1982.